Mathematical modeling of colloid and virus cotransport in porous media: Application to experimental data

Vasileios E. Katzourakis [a], Constantinos V. Chrysikopoulos [b],*

[a] Environmental Engineering Laboratory, Civil Engineering Department, University of Patras, Patras 26500, Greece
[b] School of Environmental Engineering, Technical University of Crete, Chania 73100, Greece

ABSTRACT

A conceptual mathematical model was developed to describe the simultaneous transport (cotransport) of viruses and colloids in three-dimensional, water saturated, homogeneous porous media with uniform flow. The model accounts for the migration of individual virus and colloid particles as well as viruses attached onto colloids. Viruses can be suspended in the aqueous phase, attached onto suspended colloids and the solid matrix, and attached onto colloids previously attached on the solid matrix. Colloids can be suspended in the aqueous phase or attached on the solid matrix. Viruses in all four phases (suspended in the aqueous phase, attached onto suspended colloid particles, attached on the solid matrix, and attached onto colloids previously attached on the solid matrix) may undergo inactivation with different inactivation coefficients. The governing coupled partial differential equations were solved numerically using finite difference methods, which were implemented explicitly or implicitly so that both stability and speed factors were satisfied. Furthermore, the experimental data collected by Syngouna and Chrysikopoulos [1] were satisfactorily fitted by the newly developed cotransport model.

© 2014 Elsevier Ltd. All rights reserved.

1. Introduction

Mathematical modeling of contaminant, colloid and biocolloid (virus, protozoa, and bacteria) transport in subsurface formations has captured the attention of several scientists and environmental engineers, because of the increased public concern and attention paid to the disposal, movement and fate of contaminants in natural systems. Groundwater contaminated with pathogenic microorganisms has severe consequences to public health throughout the world, but particularly in small communities and developing countries, where untreated groundwater is often consumed [2]. Although waterborne diseases can be controlled, outbreaks continue to exist [3]. The majority of the waterborne diseases reported in the United States during the time period 1971–2006 were associated with cases of groundwater contamination [4]. Therefore, understanding the transport mechanisms that control biocolloid migration through subsurface formations is essential for the protection of public health.

Numerous experimental and theoretical studies have focused on factors that govern colloid and biocolloid transport in fractured and porous media [5–21]. Of particular importance is the presence of colloids suspended in the aqueous phase. It should be noted that colloids are small particles with size in the range 1 nm to 10 μm

[22] that occur naturally in practically every aquatic system due to precipitation of supersaturated phases, mobilization of existing colloidal phases, well drilling, leaching from the vadose zone, and dissolution of inorganic cementing agents that bind colloid-size materials to solid surfaces [23–26]. Colloids remain suspended in water for long time because they have low sedimentation rate, and undergo random Brownian motion while carrying surface electric charge. Many pollutants, including biocolloids, in aqueous media are readily adsorbed/attached onto colloidal particles, which often act as carriers. Several experimental and theoretical studies have shown that, depending on the physicochemical conditions of the fractured and porous media, colloids can either enhance or hinder the transport of organic and inorganic pollutants [27–45].

Several research groups have developed analytical and numerical mathematical models to describe and predict colloid and biocolloid transport in fractured and porous media [46–56]. Furthermore, a few mathematical models have been developed to describe facilitated contaminant and biocolloid transport in fractured and porous media [28,57–61].

The objective of the present study is to (a) improve the one-dimensional mathematical model for colloid-facilitated bacteria transport developed by Vasiliadou and Chrysikopoulos [61] for colloid-facilitated virus transport in three-dimensional, water saturated, homogeneous porous media with uniform flow, (b) provide an efficient numerical solution to the newly developed virus–colloid cotransport model, and (c) apply the numerical model to

* Corresponding author. Tel.: +30 28210 37797; fax: +30 28210 37847.
  E-mail address: cvc@enveng.tuc.gr (C.V. Chrysikopoulos).

Nomenclature

C_i	concentration of suspended species i, M/L^3
C_i^*	concentration of species i attached onto the solid matrix, M_i/M_s
C_c	concentration of suspended colloids, M_c/L^3
C_c^*	concentration of colloids attached onto the solid matrix, M_c/M_s
C_v	concentration of suspended viruses, M_v/L^3
C_v^*	concentration of viruses attached onto the solid matrix, M_v/M_s
C_{vc}	concentration of viruses attached onto suspended colloid particles, M_v/M_c
C_{vc}^*	concentration of virus–colloid particles attached onto the solid matrix, M_v/M_c
$C_c^{*(r)}$	concentration of colloids reversibly attached onto the solid matrix, M_c/M_s
$C_c^{*(i)}$	concentration of colloids irreversibly attached onto the solid matrix, M_c/M_s
C_{oi}	initial concentration of suspended species i, M_i/L^3
D_{xi}	longitudinal hydrodynamic dispersion coefficient of species i, L^2/t
D_{yi}	lateral hydrodynamic dispersion coefficient of species i, L^2/t
D_{zi}	vertical hydrodynamic dispersion coefficient of species i, L^2/t
$\mathcal{D}_{ei}$	effective diffusion coefficient of species i, L^2/t
$\mathcal{D}_{iw}$	molecular diffusion coefficient of species i in fluid w (water), L^2/t
F_c	general form of colloids source configuration, $M_c/L^3 t$
F_v	general form of viruses source configuration, $M_v/L^3 t$
i	species c = colloid, v = virus, vc = virus–colloid
L_x	length of porous medium (packed column), L
L_y	width of porous medium, L
L_z	height of porous medium, L
L	length, L
M_c	mass of colloids, M_c
M_s	mass of the solid matrix, M_s
M_v	mass of viruses, M_v
n_x	number of discretization unit cells in the x-direction, (–)
Q	flow rate, L^3/t
$r_{c-c^{*(i)}}$	rate coefficient of irreversible colloid attachment onto the sold matrix, $1/t$
$r_{c^{*(r)}-c}$	rate coefficient of reversible colloid detachment from the solid matrix, $1/t$
$r_{c-c^{*(r)}}$	rate coefficient of reversible colloid attachment onto the sold matrix, $1/t$
r_{v-v^*}	rate coefficient of virus attachment onto the solid matrix, $1/t$
r_{v^*-v}	rate coefficient of virus detachment from the solid matrix, $1/t$

r_{v-vc}	rate coefficient of virus attachment onto suspended colloid particles, $L^3/M_c t$
r_{vc-v}	rate coefficient of virus detachment from suspended colloid particles, $1/t$
$r_{v-v^*c^*}$	rate coefficient of virus attachment onto colloid particles already attached ontothe solid matrix, $L^3/M_c t$
$r_{vc-v^*c^*}$	rate coefficient of virus–colloid particle attachment onto the solid matrix, $1/t$
$r_{v^*c^*-v}$	rate coefficient of virus detachment from colloid particles attached onto the solid matrix, $1/t$
$r_{v^*c^*-vc}$	rate coefficient of virus–colloid particle detachment from the solid matrix, $1/t$
t	time, t
t_p	injection time period, t
U	interstitial velocity, L/t
X	spatial coordinate in the longitudinal direction, L
Y	spatial coordinate in the lateral direction, L
Z	spatial coordinate in the vertical direction, L

Greek letters

α_L	longitudinal dispersivity, L
α_{T_y}	transverse (lateral) dispersivity, L
α_{T_z}	transverse (vertical) dispersivity, L
$\delta(x)$	Dirac delta function, $1/L$
θ	porosity of the column material, (L^3 voids)/(L^3 solid matrix)
λ_v	decay rate of viruses suspended in the liquid phase, $1/t$
λ_v^*	decay rate of viruses sorbed or attached onto the solid matrix, $1/t$
λ_{vc}	decay rate of virus–colloid complexes suspended in the liquid phase, $1/t$
λ_{vc}^*	decay rate of virus–colloid complexes sorbed or attached onto the solid matrix, $1/t$
Λ_{v-vc}	mass accumulation rate due to attachment of suspended viruses onto suspended colloid particles, $M_v/L^3 t$
$\Lambda_{v-v^*c^*}$	mass accumulation rate due to attachment of suspended viruses onto colloid particles already attached onto the solid matrix, $M_v/L^3 t$
Λ_{vc-v}	mass accumulation rate due to virus detachment from suspended colloid particles, $M_v/L^3 t$
$\Lambda_{v^*c^*-v}$	mass accumulation rate due to virus detachment from colloid particles attached onto the solid matrix, $M_v/L^3 t$
$\Lambda_{vc-v^*c^*}$	mass accumulation rate due to attachment of suspended virus–colloid particles onto the solid matrix, $M_v/L^3 t$
$\Lambda_{v^*c^*-vc}$	mass accumulation rate due to detachment of virus–colloid particles from the solid matrix, $M_v/L^3 t$
ρ_b	bulk density of the solid matrix, M_s/L^3
τ^*	tortuosity, (–)

the experimental data for bacteriophage (MS2, ΦX174) and clay (kaolinite, montmorillonite) cotransport, published by Syngouna and Chrysikopoulos [1]. To our knowledge no other three-dimensional colloid and virus cotransport model together with its efficient and robust numerical solution has neither been presented in the literature nor has been employed to available experimental data before.

2. Model development

The proposed colloid facilitated virus transport model assumes that the colloids partition between the aqueous phase and the solid matrix, while viruses may attach onto colloidal particles in the aqueous phase, onto the solid matrix, and onto colloids previously at-

tached onto the solid matrix. Consequently, colloid particles can be suspended in the aqueous phase C_c [M_c/L^3], or attached onto the solid matrix C_c^* [M_c/M_s]. Viruses can be suspended in the aqueous phase C_v [M_v/L^3], directly attached onto the solid matrix C_v^* [M_v/M_s], attached onto suspended colloid particles (virus–colloid particles) C_{vc} [M_v/M_c], and attached onto colloid particles already attached onto the solid matrix (or equivalently virus–colloid particles attached onto the solid matrix) C_{vc}^* [M_v/M_c]. A schematic illustration of the various types of concentrations considered in the present mathematical model is given in Fig. 1. To simplify the notation, the various masses are indicated as follows: M_c is the mass of colloids, M_v is the mass of viruses, and M_s is the mass of the solid matrix. Also, the subscripts c, v, and vc represent colloid, virus and virus–colloid, respectively.
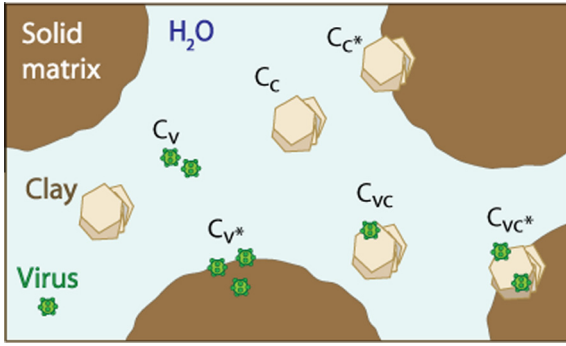
Fig. 1. Schematic illustration of the various concentrations accounted for in the cotransport numerical model.

2.1. Colloid transport equations

The transport of suspended colloid particles in three-dimensional saturated, homogeneous porous media with uniform flow, accounting for nonequilibrium attachment onto the solid matrix, is governed by the following partial differential equation [62,63]:

$$\frac{\partial C_c(t,x,y,z)}{\partial t} + \frac{\rho_b}{\theta}\frac{\partial C_c^*(t,x,y,z)}{\partial t} - D_{xc}\frac{\partial^2 C_c(t,x,y,z)}{\partial x^2} - D_{yc}\frac{\partial^2 C_c(t,x,y,z)}{\partial y^2}$$
$$- D_{zc}\frac{\partial^2 C_c(t,x,y,z)}{\partial z^2} + U\frac{\partial C_c(t,x,y,z)}{\partial x} = F_c(t,x,y,z) \quad (1)$$

where U [L/t] is the average interstitial velocity; t [t] is time; ρ_b [M_s/L^3] is the bulk density of the solid matrix; θ [–] is the porosity of the porous medium; x [L] is the spatial coordinate in the longitudinal direction; y [L] is the spatial coordinate in the lateral direction; z [L] is the spatial coordinate in the vertical direction; $F_c(t,x,y,z)$ [M_c/L^3t] is a general form of the colloid source configuration; and D_{xi}, D_{yi}, D_{zi} [L^2/t] are the longitudinal, lateral, and vertical hydrodynamic dispersion coefficients, respectively, of the suspended species i ($i = c, v, vc$), which are defined as:

$$D_{xi} = \alpha_L U + \mathcal{D}_{ei} \quad (2)$$

$$D_{yi} = \alpha_{T_y} U + \mathcal{D}_{ei} \quad (3)$$

$$D_{zi} = \alpha_{T_z} U + \mathcal{D}_{ei} \quad (4)$$

where $\alpha_L, \alpha_{T_y}, \alpha_{T_z}$ [L] are the longitudinal, transverse (lateral), and transverse (vertical) dispersivities, respectively; and $\mathcal{D}_{ei} = \mathcal{D}_{iw}/\tau^*$ [L^2/t] is the effective molecular diffusion coefficient of the suspended species i ($\tau^* \geqslant 1$ [–] is the tortuosity coefficient, and $\mathcal{D}_{iw}$ [L^2/t] is the molecular diffusion coefficient of the suspended species i in fluid w, which is assumed to be water).

The colloids attached onto the solid matrix, C_c^*, may be reversibly attached, $C_c^{*(r)}$ [M_c/M_s], and/or irreversibly attached, $C_c^{*(i)}$ [M_c/M_s]. Therefore, the concentration of colloids attached onto the solid matrix is the sum of the reversibly and irreversibly attached colloid concentrations:

$$C_c^* = C_c^{*(r)} + C_c^{*(i)} \quad (5)$$

Consequently, the corresponding colloid accumulation term in (1) is expressed as:

$$\frac{\partial C_c^*(t,x,y,z)}{\partial t} = \frac{\partial C_c^{*(r)}(t,x,y,z)}{\partial t} + \frac{\partial C_c^{*(i)}(t,x,y,z)}{\partial t} \quad (6)$$

The reversible colloid accumulation term is described by the following nonequilibrium equation [62,63]:

$$\frac{\rho_b}{\theta}\frac{\partial C_c^{*(r)}(t,x,y,z)}{\partial t} = r_{c-c^{*(r)}}C_c(t,x,y,z) - r_{c^{*(r)}-c}\frac{\rho_b}{\theta}C_c^{*(r)}(t,x,y,z) \quad (7)$$

where $r_{c-c^{*(r)}}$ [$1/t$] is the rate coefficient of reversible colloid attachment onto the solid matrix, and $r_{c^{*(r)}-c}$ [$1/t$] is the rate coefficient of reversible colloid detachment from the solid matrix; whereas the irreversible accumulation term is described by the following non-equilibrium equation [26]:

$$\frac{\rho_b}{\theta}\frac{\partial C_c^{*(i)}(t,x,y,z)}{\partial t} = r_{c-c^{*(i)}}C_c(t,x,y,z) \quad (8)$$

where $r_{c-c^{*(i)}}$ [$1/t$] is the rate coefficient of irreversible colloid attachment onto the solid matrix.

2.2. Colloid facilitated virus transport equations

The transport of suspended viruses in three-dimensional water saturated porous media, accounting for virus attachment onto (a) the solid matrix, (b) suspended colloid particles, and (c) colloid particles already attached onto the solid matrix, as well as for first-order decay (inactivation) of suspended and attached viruses with different decay rates, is governed by the following partial differential equation [28,57,61]:

$$\frac{\partial}{\partial t}\left(C_v + \frac{\rho_b}{\theta}C_v^* + C_c C_{vc} + \frac{\rho_b}{\theta}C_c^* C_{vc}^*\right)$$
$$= D_{xv}\frac{\partial^2 C_v}{\partial x^2} + D_{xvc}\frac{\partial^2}{\partial x^2}(C_c C_{vc}) + D_{yv}\frac{\partial^2 C_v}{\partial y^2} + D_{yvc}\frac{\partial^2}{\partial y^2}(C_c C_{vc})$$
$$+ D_{zv}\frac{\partial^2 C_v}{\partial z^2} + D_{zvc}\frac{\partial^2}{\partial z^2}(C_c C_{vc}) - U\frac{\partial}{\partial x}(C_v + C_c C_{vc}) - \lambda_v C_v$$
$$- \lambda_{vc}C_v C_{vc} - \lambda_v^*\frac{\rho_b}{\theta}C_v^* - \lambda_{vc}^*\frac{\rho_b}{\theta}C_c^* C_{vc}^* + F_v(t,x,y,z) \quad (9)$$

where λ_v [$1/t$] is the decay rate of viruses suspended in the aqueous phase; λ_v^* [$1/t$] is the decay rate of viruses attached onto the solid matrix; λ_{vc} [$1/t$] is the decay rate of virus–colloid particles suspended in the aqueous phase, which also accounts for irreversible attachment of virus–colloid particles onto the solid matrix; λ_{vc}^* [$1/t$] is the decay rate of virus–colloid particles attached onto the solid matrix; and $F_v(t,x,y,z)$ [M_v/L^3t] is a general form of the viruses source configuration. Assuming that there is minimum interaction between C_v and $C_c^{*(i)}$, or equivalently negligible attachment of suspended viruses onto colloids irreversibly attached onto the solid matrix, it is reasonable to assume that the relationship $C_c^* = C_c^{*(r)}$ is valid for the colloid facilitated virus transport model.

The second mass accumulation rate that appears on the left side of (9) is described by the following nonequilibrium relation [62,63]:

$$\frac{\rho_b}{\theta}\frac{\partial C_v^*(t,x,y,z)}{\partial t} = r_{v-v^*}C_v(t,x,y,z) - r_{v^*-v}\frac{\rho_b}{\theta}C_v^*(t,x,y,z)$$
$$- \lambda_v^*\frac{\rho_b}{\theta}C_v^*(t,x,y,z) \quad (10)$$

where r_{v-v^*} [$1/t$] is the rate coefficient of virus attachment onto the solid matrix, and r_{v^*-v} [$1/t$] is the rate coefficient of virus detachment from the solid matrix.

The third mass accumulation rate that appears on the left side of (9) can be expressed as [60]:

$$\frac{\partial}{\partial t}(C_c C_{vc}) = \Lambda_{v-vc} - \Lambda_{vc-v} + \Lambda_{v^*c^*-vc} - \Lambda_{vc-v^*c^*} - \lambda_{vc}C_c C_{vc} \quad (11)$$

The term Λ_{v-vc} [M_v/L^3t] is the mass accumulation rate due to attachment of suspended viruses onto suspended colloid particles. The following linear relationship between virus–colloid particles, C_{vc}, and suspended virus particles, C_v, is assumed to be valid:

$$\Lambda_{v-vc} = r_{v-vc}(C_c C_v) \quad (12)$$

where r_{v-vc} [$L^3/M_c t$] is the rate coefficient of virus attachment onto suspended colloid particles; The term Λ_{vc-v} [M_v/L^3t] is the mass
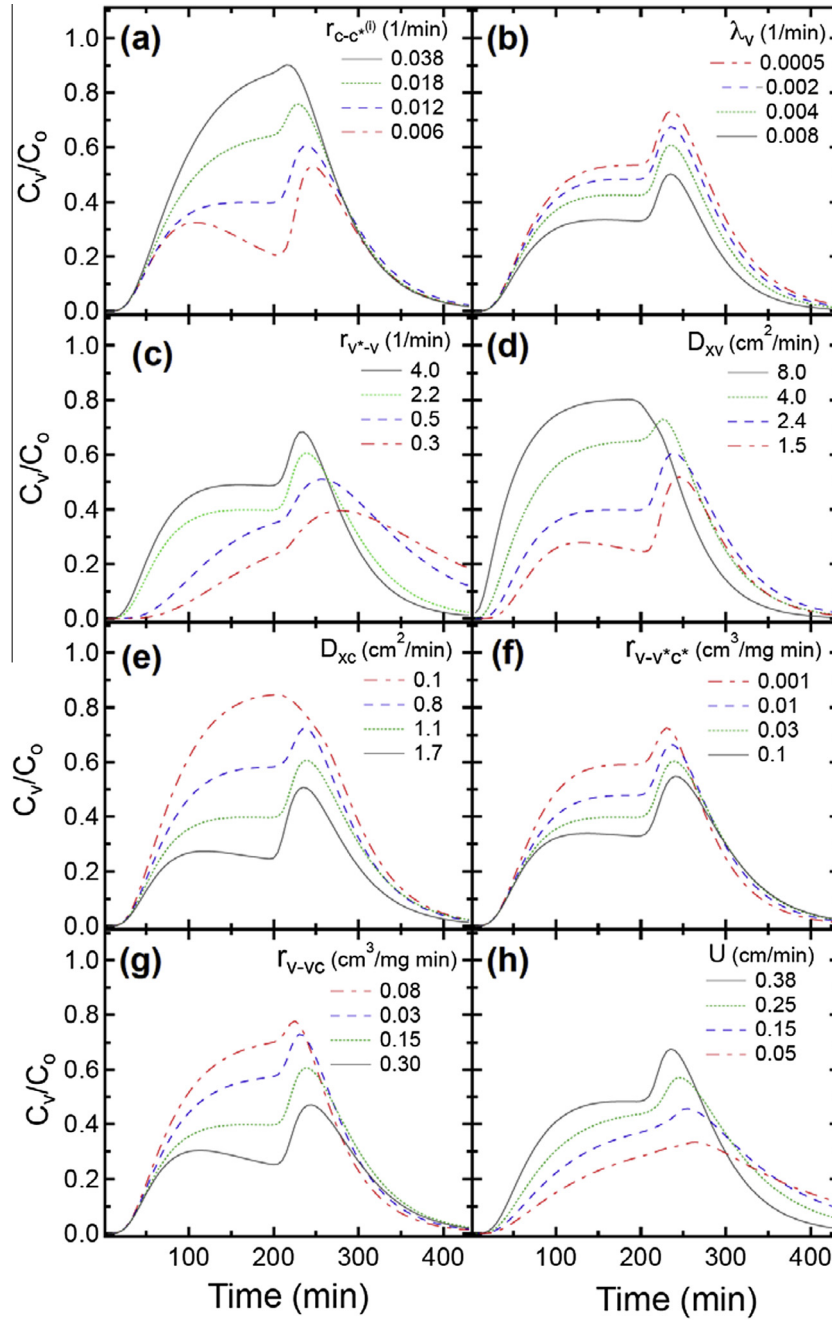
Fig. 2. Sensitivity analysis on eight different parameters of the virus–colloid cotransport model. Here $Q = 0.8$ mL/min, and $t_p = 190$ min.

accumulation rate due to virus detachment from suspended virus–colloid particles, expressed by the following linear relationship [61]:

$$\Lambda_{vc-v} = r_{vc-v}(C_c C_{vc}) \tag{13}$$

where r_{vc-v} [1/t] is the rate coefficient of virus detachment from suspended colloids; $\Lambda_{vc-v^*c^*}$ [$M_v/L^3 t$] is the mass accumulation rate due to attachment of virus colloid particles onto the solid matrix, expressed by the following linear relationship [61]:

$$\Lambda_{vc-v^*c^*} = r_{vc-v^*c^*}(C_c C_{vc}) \tag{14}$$

where $r_{vc-v^*c^*}$ [1/t] is the rate coefficient of virus–colloid particle attachment onto the solid matrix. $\Lambda_{v^*c^*-vc}$ [$M_v/L^3 t$] is the mass accumulation rate due to detachment of virus–colloid particles from the solid matrix, expressed by the following linear relationship [61]:

$$\Lambda_{v^*c^*-vc} = \frac{\rho_b}{\theta} r_{v^*c^*-vc}(C_c^* C_{vc}^*) \tag{15}$$

where $r_{v^*c^*-vc}$ [1/t] is the rate coefficient of virus–colloid particle detachment from the solid matrix. Combining Eqs. (11)–(15) yields:

$$\frac{d}{dt}(C_c C_{vc}) = r_{v-vc}C_c C_v - r_{vc-v}(C_c C_{vc}) + \frac{\rho_b}{\theta} r_{v^*c^*-vc}(C_c^* C_{vc}^*) \\ - r_{vc-v^*c^*}(C_c C_{vc}) - \lambda_{vc}C_c C_{vc} \tag{16}$$

The fourth mass accumulation rate that appears on the left side of (9) can be expressed as [60]:

$$\frac{\rho_b}{\theta}\frac{\partial}{\partial t}(C_c^* C_{vc}^*) = \Lambda_{v-v^*c^*} - \Lambda_{v^*c^*-v} + \Lambda_{vc-v^*c^*} - \Lambda_{v^*c^*-vc} - \lambda_{vc}^* \frac{\rho_b}{\theta}C_c^* C_{vc}^* \tag{17}$$
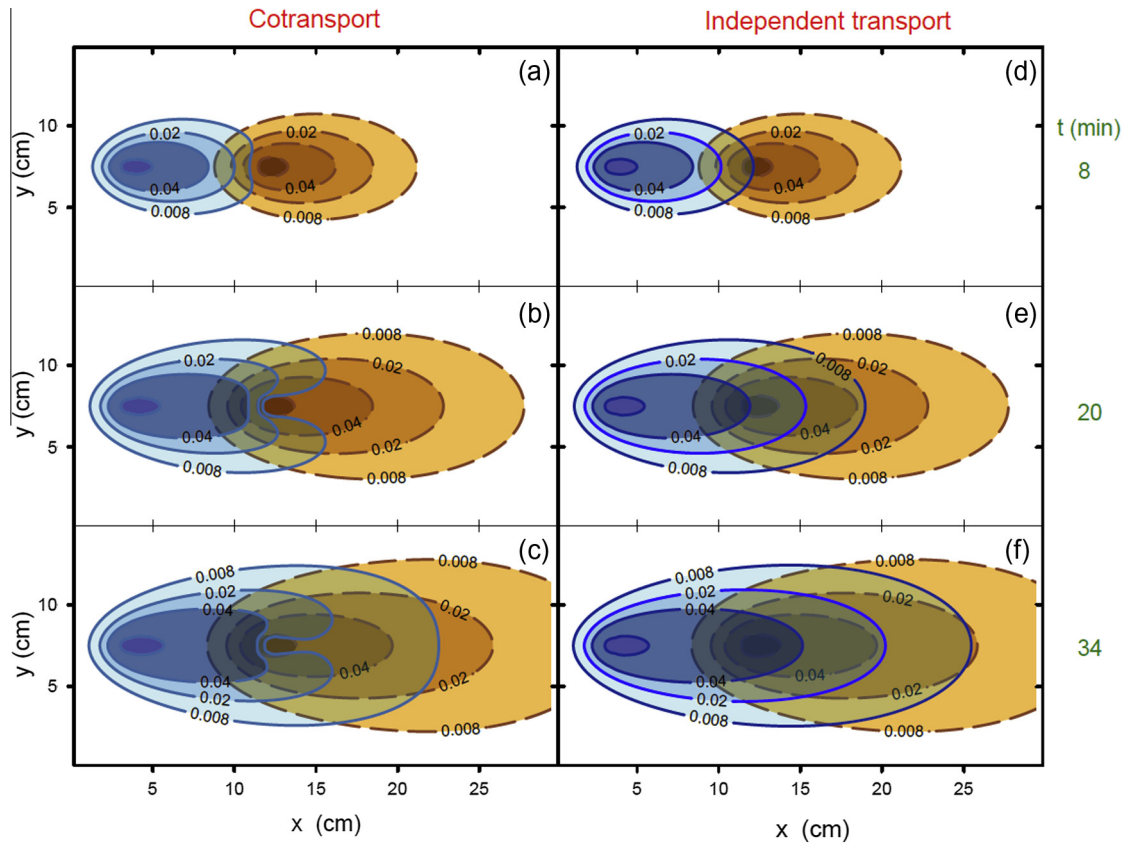
Fig. 3. Contour plots on the x–y plane of virus (solid curves) and colloid (dashed curves) normalized concentrations, for the case of (a)–(c) cotransport, and (d)–(f) independent transport in a three-dimensional porous medium at three different times, at $z = 5$ cm.

The term $\Lambda_{v-v^*c^*}$ $[M_v/L^3t]$ is the mass accumulation rate due to virus attachment onto colloids that are already attached onto the solid matrix. The following linear relationship between the virus–colloid particles attached onto the solid matrix, C_{vc}^*, and suspended virus particles, C_v, is assumed to be valid:

$$\Lambda_{v-v^*c^*} = \frac{\rho_b}{\theta} r_{v-v^*c^*} (C_c^* C_v) \tag{18}$$

where $r_{v-v^*c^*}$ $[L^3/M_c t]$ is the rate coefficient of virus attachment onto colloids already attached onto the solid matrix. $\Lambda_{v^*c^*-v}$ $[M_v/L^3t]$ is the mass accumulation rate due to virus detachment from colloids

attached onto the solid matrix, expressed by the following linear relationship [61]:

$$\Lambda_{v^*c^*-v} = \frac{\rho_b}{\theta} r_{v^*c^*-v} (C_c^* C_{vc}^*) \tag{19}$$

Table 1
Physical parameters for the cotransport experiments.[a]

	C_{ov} (pfu/mL)	C_{oc} (mg/mL)	Q (mL/min)	t_p (min)	U (cm/min)
MS2–KGa-1b					
Exp. 1	51500	62.8	0.8	190.0	0.38
Exp. 2	2425	69.1	1.5	117.0	0.74
Exp. 3	4738	63.8	2.5	75.0	1.21
ΦX174–KGa-1b					
Exp. 1	1418.4	54.3	0.8	190.0	0.38
Exp. 2	3237.5	57.4	1.5	119.0	0.74
Exp. 3	12366.6	62.8	2.5	75.0	1.21
MS2–STx-1b					
Exp. 1	406000	115.3	0.8	180.0	0.38
Exp. 2	181333	91.2	1.5	119.0	0.74
Exp. 3	520333	87.6	2.5	75.5	1.21
ΦX174–STx-1b					
Exp. 1	40000	78.5	0.8	197.0	0.38
Exp. 2	61667	78.5	1.5	121.0	0.74
Exp. 3	84800	100.7	2.5	75.0	1.21

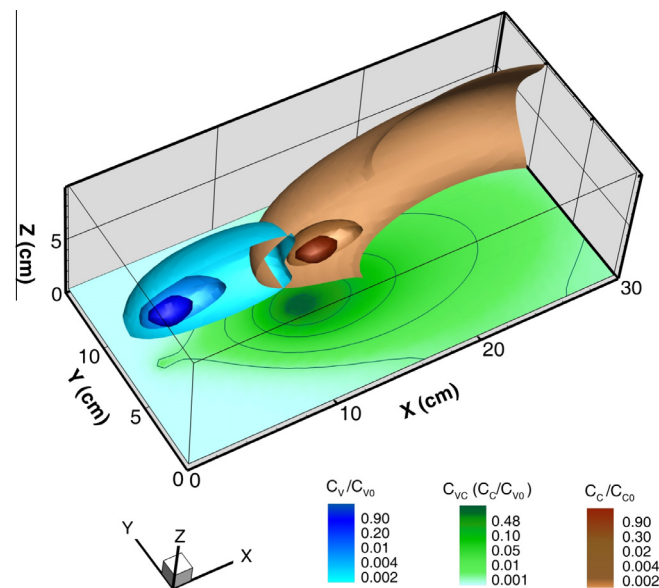[a] ($L_x = 30$ cm, $n_x = 1000$ cells, $\rho_b = 1610$ mg/cm^3, $\theta = 0.42$).

Fig. 4. Isosurface three-dimensional plots of virus (blue surfaces) and colloid (brown surfaces) normalized concentrations, along with a projected x–y plane slice at $z = 5$ cm, of the virus–colloid particles (green contour), at $t = 20$ min. (For interpretation of the references to color in this figure legend, the reader is referred to the web version of this article.)

Table 2
Parameters for the cotransport experiments.

Parameter	Status	MS2–KGa-1b			ΦX174–KGa-1b			MS2–STx-1b			ΦX174–STx-1b		
		Exp. 1	Exp. 2	Exp. 3	Exp. 1	Exp. 2	Exp. 3	Exp. 1	Exp. 2	Exp. 3	Exp. 1	Exp. 2	Exp. 3
Colloid transport													
D_{xc} (cm²/min)	SC[a]	0.3	0.7	1.0	0.3	0.7	1.0	0.3	0.7	1.0	0.3	0.7	1.0
D_{yc} (cm²/min)	Fixed	0	0	0	0	0	0	0	0	0	0	0	0
D_{zc} (cm²/min)	Fixed	0	0	0	0	0	0	0	0	0	0	0	0
$r_{c-c^{*(l)}}$ (1/min)	Fitted	0.014 ± 0.001	0.014 ± 0.001	0.03 ± 0.002	0.007 ± 0.002	0.028 ± 0.002	0.058 ± 0.002	0.013 ± 0.001	0.018 ± 0.001	0.044 ± 0.02	0.011 ± 0.004	0.040 ± 0.005	0.0396 ± 0.01
$r_{c-c^{*(r)}}$ (1/min)	VC[a]	0.037	0.006	0.045	0.01	0.078	0.081	0.025	0.013	0.047	0.015	0.293	0.132
$r_{c^{*(r)}-c}$ (1/min)	Fitted	0.12 ± 0.05	0.021 ± 0.01	0.138 ± 0.05	0.042 ± 0.002	0.112 ± 0.01	0.12 ± 0.01	0.043 ± 0.01	0.037 ± 0.01	0.087 ± 0.04	0.018 ± 0.002	0.248 ± 0.02	0.319 ± 0.06
Colloid and virus cotransport9													
D_{xv} (cm²/min)	VC[a]	0.11	0.13	0.17	0.12	0.53	0.5	0.14	0.21	0.46	0.18	0.12	0.63
D_{yv} (cm²/min)	Fixed	0	0	0	0	0	0	0	0	0	0	0	0
D_{zv} (cm²/min)	Fixed	0	0	0	0	0	0	0	0	0	0	0	0
D_{xvc} (cm²/min)	Im[b]	0.3	0.7	1.0	0.3	0.7	1.0	0.3	0.7	1.0	0.3	0.7	1.0
D_{yvc} (cm²/min)	Fixed	0	0	0	0	0	0	0	0	0	0	0	0
D_{zvc} (cm²/min)	Fixed	0	0	0	0	0	0	0	0	0	0	0	0
λ_v (1/min)	Fitted	0.014 ± 0.005	0.050 ± 0.01	0.042 ± 0.02	0.034 ± 0.005	0.016 ± 0.002	0.078 ± 0.03	0.011 ± 0.001	0.045 ± 0.02	0.054 ± 0.002	0.014 ± 0.003	0.028 ± 0.011	0.032 ± 0.011
λ_v^* (1/min)	Im[b]	0.007	0.026	0.021	0.017	0.008	0.039	0.005	0.022	0.027	0.007	0.014	0.016
λ_{vc} (1/min)	SC[a]	9.6×10^{-4}	9.63×10^{-4}	0.02	9.6×10^{-4}	0.029	0.024	0.009	0.007	0.057	0.009	0.007	0.057
λ_{vc}^* (1/min)	SC[a]	4.8×10^{-4}	4.81×10^{-4}	0.01	4.8×10^{-4}	0.014	0.012	0.004	0.004	0.028	0.004	0.004	0.029
r_{v-v^*} (1/min)	SC[a]	0.087	0.650	0.096	8.0×10^{-4}	0.076	0.057	0.023	0.019	0.001	0.001	0.223	0.245
r_{v^*-v} (1/min)	Fitted	0.6 ± 0.2	0.54 ± 0.2	0.017 ± 0.01	3.54 ± 1.5	0.067 ± 0.02	0.52 ± 0.2	0.058 ± 0.02	0.096 ± 0.04	0.490 ± 0.25	0.236 ± 0.08	0.553 ± 0.07	1.83 ± 0.2
r_{v-vc} (cm³/ mg min)	Fitted	0.002 ± 0.001	0.015 ± 0.001	0.063 ± 0.001	0.009 ± 0.002	0.34 ± 0.08	0.08 ± 0.006	0.038 ± 0.02	0.077 ± 0.05	0.09 ± 0.04	0.012 ± 0.001	0.013 ± 0.003	0.015 ± 0.001
r_{vc-v} (1/min)	Im[b]	0.069	0.022	0.050	0.071	0.039	0.210	0.078	0.025	0.248	0.069	0.053	0.480
$r_{v-v^*c^*}$ (cm³/ mg min)	Im[b]	0.002	0.015	0.063	0.009	0.34	0.08	0.038	0.077	0.09	0.012	0.013	0.015
$r_{vc-v^*c^*}$ (1/min)	VC[a]	0.002	0.001	0.005	1.3×10^{-4}	0.027	0.014	0.003	0.009	0.077	0.001	0.2038	0.058
$r_{v^*c^*-v}$ (1/min)	VC[a]	0.069	0.022	0.050	0.071	0.039	0.210	0.078	0.025	0.248	0.069	0.053	0.480
$r_{v^*c^*-vc}$ (1/min)	VC[a]	0.049	0.06	0.038	0.045	0.07	0.001	0.060	0.055	0.050	0.045	0.740	0.060

[a] VC – Vasiliadou and Chrysikopoulos [61]; SC – Syngouna and Chrysikopoulos [17].
[b] Im – Imposed.

Table 3
Parameter values used in the numerical solution.

Number of cells	500–1000
Temporal discretization step (δt) (min)	0.01–0.05
Spatial discretization step (δx) [cm]	0.03–0.06
Peclet Number	<2
Crout Number	<1
Relative tolerance in main solver controlled by δx and δt	0.05
Relative tolerance between iterations for a particular δt	10^{-5}
ODE solver Relative tolerance	10^{-8}
ODE solver Absolute tolerance	10^{-35}

where $r_{v^*c^*-v}$ [1/t] is the rate coefficient of virus detachment from virus–colloid particles attached onto the solid matrix. Combining Eqs. (14), (15), (17), (18), and (19) yields:

$$\frac{\rho_b}{\theta}\frac{d}{dt}(C_c^*C_{vc}^*) = \frac{\rho_b}{\theta}r_{v-v^*c^*}(C_c^*C_v) - \frac{\rho_b}{\theta}r_{v^*c^*-v}(C_c^*C_{vc}^*)$$
$$+ r_{vc-v^*c^*}(C_cC_{vc}) - \frac{\rho_b}{\theta}r_{v^*c^*-vc}(C_c^*C_{vc}^*) - \lambda_{vc}^*\frac{\rho_b}{\theta}C_c^*C_{vc}^* \quad (20)$$

2.3. Initial and boundary conditions

The initial condition and the appropriate boundary conditions for a three-dimensional confined aquifer with finite dimensions are as follows:

$$C_i(0, x, y, z) = 0 \quad (21)$$

$$-D_{xi}\frac{\partial C_i(t, 0, y, z)}{\partial x} + UC_i(t, 0, y, z) = \begin{cases} UC_{oi}, & t \leqslant t_p \\ 0, & t > t_p \end{cases} \quad (22)$$

$$\frac{\partial C_i^2(t, L_x, y, z)}{dx^2} = 0 \quad (23)$$

$$\frac{\partial C_i(t, x, 0, z)}{\partial y} = \frac{\partial C_i(t, x, L_y, z)}{\partial y} = 0 \quad (24)$$

$$\frac{\partial C_i(t, x, y, 0)}{\partial z} = \frac{\partial C_i(t, x, y, L_z)}{\partial z} = 0 \quad (25)$$

where the subscript i represents either viruses ($i = v$) or clay colloids ($i = c$); $L_x, L_y, L_y, [L]$ are the length, width, and height of the porous medium, respectively; C_{oi} is the initial constant aqueous phase concentration of species i (virus or colloids), and t_p [t] is the time period over which colloids and viruses are injected (inserted) in the porous medium. Condition (21) establishes that there is no initial concentration of species i within the three-dimensional porous medium. The third-type boundary condition (22), which assures mass conservation, implies a constant mass flux of species i at the inlet ($x = 0$) over the injection time period [64]. The downstream boundary condition (23) preserves concentration slope continuity for the finite length aquifer [65]. Conditions (24) and (25) imply that there is no flux of species i across the lateral and vertical boundaries of the confined aquifer. Note that the initial and boundary conditions (21)–(25) are applied twice: first to the colloid transport equation (1), and then to the virus–colloid cotransport equation (9). Finally, the use of boundary condition (22) imposes that $F_c(t, x, y, z) = F_v(t, x, y, z) = 0$.

3. Numerical procedures

For the solution of the newly developed mathematical model described in the previous section, the classical finite difference
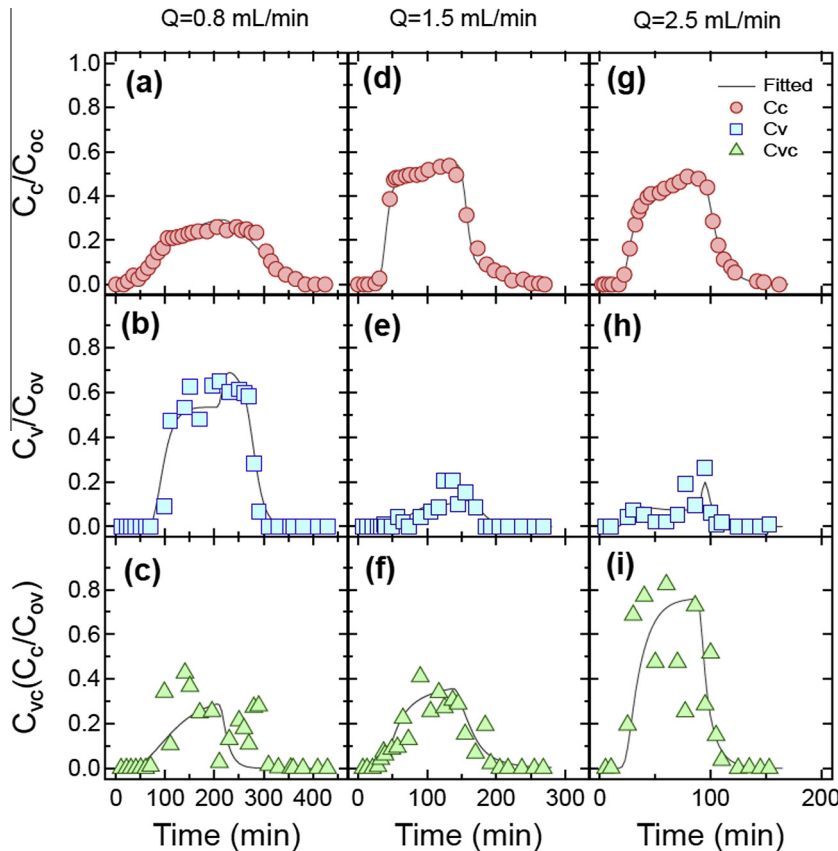

Fig. 5. Breakthrough data of normalized (a), (d) and (g) C_c, (b), (e) and (h) C_v, and (c), (f) and (i) C_{vc} from cotransport experiments with MS2 and KGa-1b conducted by Syngouna and Chrysikopoulos [1] in columns packed with glass beads (symbols) and fitted model simulations (solid curves).
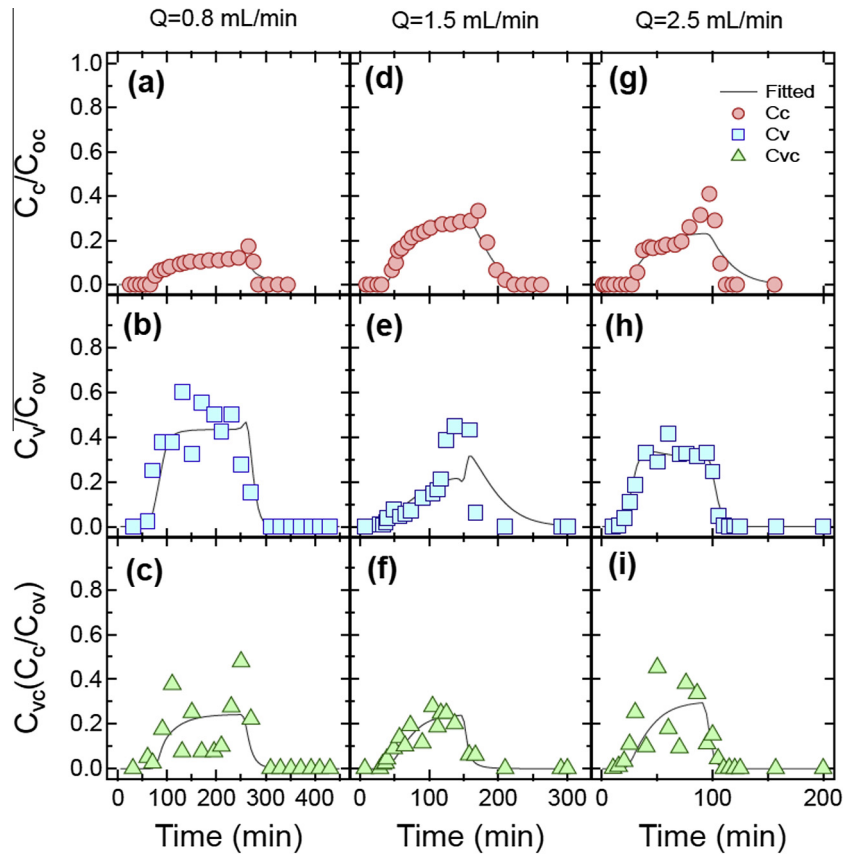
Fig. 6. Breakthrough data of normalized (a), (d) and (g) C_c, (b), (e) and (h) C_v, and (c), (f) and (i) C_{vc} from cotransport experiments with ΦX174 and KGa-1b conducted by Syngouna and Chrysikopoulos [1] in columns packed with glass beads (symbols) and fitted model simulations (solid curves).

method was chosen and implemented in the semi-implicit fashion as required by the Crank–Nikolson scheme. The resulting large system of linear equations was treated with the Pardiso package, which is a thread-safe, and memory efficient software able to solve sparse symmetric and asymmetric linear systems of equations. High performance is ensured by distributing computational load over a number of individual processors on shared-memory and distributed-memory systems [66]. In order to solve Eqs. (16) and (20), the arising numerical difficulties due to the existence of stiffness must be resolved. Note that a system of ordinary differential equations is considered "stiff" when the various components of the solution evolve on markedly different time scales. Certainly, ignoring high frequency components of the solution leads to erroneous results. Note that in (16) and (20), the concentration C_c^* (low frequency component) can take values three orders of magnitude smaller than C_c (high frequency component). The stiffness problem must be treated with extra care because it can really slow down or even prevent any possible numerical solution. For this reason, a specialized subroutine (dodesol, Intel® Ordinary Differential Equations Solver Library) capable of solving systems of ordinary differential equations (ode) with a variable or a priori unknown stiffness was employed in this work. In particular the explicit or implicit scheme was automatically chosen for every step and if necessary the numerical Jacobi matrix was computed. This way both stability and speed requirements were satisfied. The unknown variables of the numerical model presented are six: C_c, C_c^*, C_{vc}, C_{vc}^*, C_v and C_v^*. To explicitly solve for all six unknowns, a six by six system of equations must be formed, which rapidly increases the required matrix size and thus the number of calculations. However, in this study an alternative procedure was employed. Three sets of equations, consisting of two by two systems of equations, where formed, which

were solved in an iterative manner. Note that the two solution procedures produce exactly the same results, but the proposed alternative procedure provides greater speed with lower memory requirements. The systems were solved as follows: (i) Eqs. (1), (6)–(8) where solved simultaneously by the semi implicit Crank–Nicolson method in order to determine C_c, and C_c^*. (ii) these C_c and C_c^* concentrations were used in (9) and (10), which were solved together with the Pardiso solver in order to get initial estimates for C_v and C_v^*. (iii) The estimates C_v and C_v^* along with the previously calculated C_c and C_c^*, were used in the system of coupled equations (16) and (20), which was solved with the Intel® ode solver to obtain initial estimates for C_{vc} and C_{vc}^*. (iv) The estimated C_{vc} and C_{vc}^* values where fed back to step (ii) in order to produce better estimates for C_v and C_v^*, which in turn where employed in step (iii) to improve C_{vc} and C_{vc}^* estimates. (v) Steps (ii) through (iv) where repeated till all of the C_{vc}, C_{vc}^*, C_v and C_v^* values provided by successive iterations did not differ more than 5%.

The above steps were repeated sequentially until all unknown concentrations were calculated for the required time period. It should also be noted that for the numerical simulations presented in this study, each physical model was discretized into a number of cells, n_x, which was kept as low as possible to produce fast solutions, but high enough to allow for a quite small relative error (1–5%).

4. Model simulations and sensitivity analysis

To illustrate how the model parameters affect the breakthrough C_v/C_{ov} concentration curve, eight different simulations where performed and presented in Fig. 2. Clearly, the breakthrough curves for C_v/C_{ov} exhibit higher peaks as the values of $r_{c-c^{*(i)}}$, r_{v^*-v},
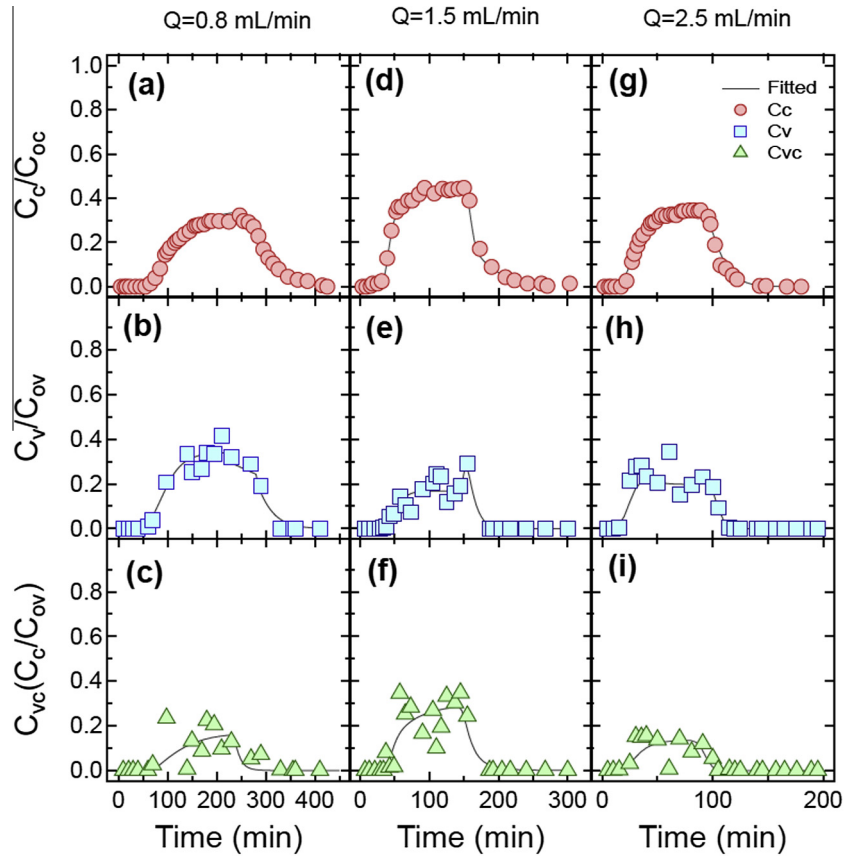
Fig. 7. Breakthrough data of normalized (a), (d) and (g) C_c, (b), (e) and (h) C_v, and (c), (f) and (i) C_{vc} from cotransport experiments with MS2 and STx-1b conducted by Syngouna and Chrysikopoulos [1] in columns packed with glass beads (symbols) and fitted model simulations (solid curves).

D_{xv}, U increase or the values of λ_v, r_{v-vc}, $r_{v-v^*c^*}$ and D_{xc} decrease. It should be noted that an increase in C_c causes C_{vc} to increase, and consequently C_v to decrease. Therefore, the trend of the simulated breakthrough curves in Fig. 2a is governed by the increase in $r_{c-c^{*(i)}}$, which causes C_c to decrease and C_v to increase. Exactly the opposite trend is observed in Fig. 2e because increasing D_{xc} causes C_c to increase or equivalently C_v to decrease. The trend of the simulated breakthrough curves in Fig. 2h is expected because decreasing U, reduces the virus travel distance in the aquifer, which in turn leads to smaller C_v at downstream locations. Fig 2c clearly shows that C_v increases with increasing r_{v^*-v}. Exactly the opposite trend is observed in Fig. 2b because λ_v controls the inactivation of viruses suspended in the liquid phase, and a decrease in λ_v causes C_v to increase. Similarly, Figs. 2g and f show that a decrease in either of the parameters r_{v-vc} and $r_{v-v^*c^*}$ leads to increasing C_v concentrations. This result is intuitive, because these two rate coefficients control virus attachment onto suspended colloid particles, and onto the solid matrix, respectively. Decreasing either of these two rate coefficients leads to higher suspended virus concentrations. Also, the trend of the simulated breakthrough curves in Fig. 2d suggests that increasing D_{xv} leads to increasing C_v. Note that several normalized virus breakthrough curves in Fig. 2 exhibit relatively sharp concentration peaks. These peaks are observed at $t > t_p$, when clean water enters the porous medium and previously created C_v^* and/or C_{vc} are converted back C_v with rates r_{v^*-v} and/or r_{vc-v}, causing a temporary but rapid increase in C_v.

In order to visualize how the colloid and virus cotransport can differ from independent colloid and virus transport, model simulations were conducted for the hypothetical case where a virus and a colloid source exist in a three-dimensional porous medium with dimensions: $L_x = 30$ cm, $L_y = 15$ cm, and $L_z = 10$ cm. The virus source is a continuous point source located at $(x,y,z) = (2.5, 7.45, 5$ cm):

$$F_v(t,x,y,z) = 1\delta(x-2.50)\delta(y-7.45)\delta(z-5)\frac{\text{pfu}}{\text{mL min}} \quad (26)$$

whereas the colloid source is a continuous circular source with radius 0.3 cm and center located at $(x,y,z) = (12, 7.45, 5$ cm):

$$F_c(t,x,y,z) = 1\delta(z-5)\frac{\text{mg}}{\text{mL min}} \quad \forall \frac{(x-12)^2}{0.3^2} + \frac{(y-7.45)^2}{0.3^2} \leqslant 1 \quad (27)$$

where δ is the Dirac delta function. All necessary model parameter-values are obtained from the literature [1], and the resulting model simulations are presented in the form of contour plots in Fig. 3 at three different times. Figs. 3a–c represent the cotransport case, whereas Figs. 3d–f represent the independent transport case, where no interaction between virus and colloid particles is allowed. Moreover, three-dimensional iso-surface plots of the cotransport case presented in contour plot of Fig. 3b are illustrated in Fig. 4. Clearly, the interaction between viruses and colloids affects significantly the migration of suspended viruses due to the formation of C_{vc} or C_{vc}^* complexes.

5. Application to experimental data

5.1. Available experimental data

Experimental data from several cotransport experiments reported by Syngouna and Chrysikopoulos [1] were used to test the accuracy of the newly developed mathematical model. In brief, bacteriophages MS2 and ΦX174 were used as model viruses, and kaolinite (KGa-1b) and montmorillonite (STx-1b) as model clay colloids. Therefore, four different virus–colloid combinations (MS2–KGa-1b, ΦX174–KGa-1b, MS2–STx-1b, ΦX174–STx1b) were
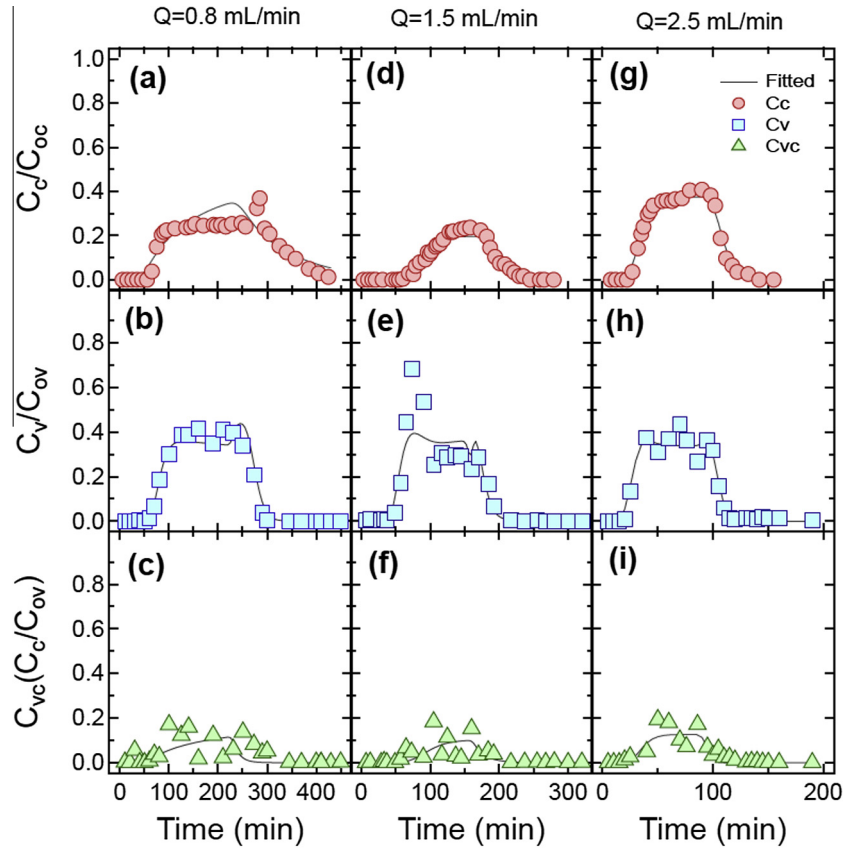
Fig. 8. Breakthrough data of normalized (a), (d) and (g) C_c, (b), (e) and (h) C_v, and (c), (f) and (i) C_{vc} from cotransport experiments with ΦX174 and STx-1b conducted by Syngouna and Chrysikopoulos [1] in columns packed with glass beads (symbols) and fitted model simulations (solid curves).

examined, and three different flow rates, Q [L^3/t], were used. All experiments were conducted in a 30 cm long glass column with 2.5 cm diameter, which was packed with 2 mm diameter glass beads. The packed column was placed horizontally to minimize gravity effects and it was fully saturated with sterile distilled deionized water. Viruses and colloids were simultaneously injected with a peristaltic pump into the column over a time period t_p. Samples were collected at the end of the column at regular time intervals and immediately were prepared for concentration determination. The bacteriophages were assayed by the double-layer overlay method, whereas the clay concentrations were determined by a UV–vis spectrophotometer. The experimental conditions are described in Table 1. Moreover, for additional experimental details refer to the work by Syngouna and Chrysikopoulos [1].

5.2. Fitting the data

The software Pest was used to fit the cotransport model to the experimental data. Pest is a stand-alone package that employs the Gauss Marquardt Levenberg with Broyden Jacobian updating method [67], and is capable of estimating multiple unknown parameters together with their confidence intervals, even for nonlinear models.

Fitting a nonlinear mathematical model to experimental data is not a trivial task. Ratha et al. [68] examined the case of one-dimensional virus transport in porous media and reported that it is not possible to simultaneously estimate the parameters D_{xv}, λ_v, λ_v^* and r_{v-v^*} uniquely. If the number of fitted parameters is three or less, the inverse procedure is expected to provide unique estimates. However, for the mathematical model used in this study, λ_v and λ_v^* tend to be incompatible with each other due to the existence of local minima in the parametric $\lambda_v - \lambda_v^*$ space, which lead

to non-unique calculation of λ and λ^* [68]. This problem can be avoided only if one of the two inactivation-rate coefficients is known a priori.

For the fitting needs of this study, the number of unknown model parameters was reduced by using the frequently employed assumption that $\lambda_v = 2\lambda_v^*$ and $\lambda_{vc} = 2\lambda_{vc}^*$ [69]. It was also assumed that colloid particles and virus–colloid complexes do not differ vastly in size, so that their hydrodynamic characteristics are similar ($D_{xc} \approx D_{xvc}$). Furthermore, it was assumed that interactions of viruses with suspended colloids do not differ significantly from interactions of viruses with colloids already attached onto the solid matrix ($r_{v-vc} \approx r_{v-v^*c^*}$ and $r_{vc-v} \approx r_{v^*c^*-v}$). Note that the cotransport model equations are backwards dependent, so that the coupled equations (9), (10), (16), and (20), which produce the C_{vc}, C_{vc}^*, C_v and C_v^* concentrations, are based only on the results provided from coupled equations (1), (6)–(8), which independently calculate C_c and C_c^*. Moreover, for every cotransport experiment, three concentration histories were provided: (i) C_c, (ii) C_{vc}, and (iii) C_v [1]; thus, the concentration histories can be fitted by the appropriate coupled system of model equations to uniquely estimate up to three model parameters. Consequently, sequential fitting was achievable and the total number of fitted parameters was reduced to 5. So first $r_{c-c^*(i)}$, and $r_{c^*(r)-c}$ were obtained from (1) and (6)–(8) using the C_c concentration history. Then, r_{v-vc}, r_{v^*-v}, and λ_v were obtained from (9), (10), (16), and (20) using the C_{vc} and C_v concentration history along with the previously estimated values for C_c and C_c^*. The rest unknown parameters (see Table 2) were fixed to reasonable values as reported in the literature. Finally, additional parameter values required by the fitting process are listed in Table 3.

The fitted parameters for all virus–colloid combinations examined in this study are listed in Table 2. Also, the experimental data together with the corresponding fitted model simulations for

MS2–KGa-1b cotransport are shown in Fig. 5, for Φ174–KGa-1b cotransport are shown in Fig. 6, for MS2–STx-1b cotransport are shown in Fig. 7, and for ΦX174–STx-1b cotransport are shown in Fig. 8. All predicted concentration histories were obtained by the numerical cotransport model using the best-fitted parameter values. Clearly, it is evident from Figs. 5–8 that there is relatively good agreement between the provided experimental data and the numerical solution. Note that the two bacteriophages used in this study (MS2 in Figs. 5 and 7 and ΦX174 in Figs. 6 and 8) have quite deferent structure, surface characteristics, and isoelectric point [21]. Nonetheless, the newly developed cotransport numerical model successfully captures the various physicochemical processes taking place during all four virus-clay cotransport cases considered in this study.

6. Summary

A new mathematical model describing the cotransport of viruses and colloids in three-dimensional, homogeneous, water saturated porous media was developed. The model was solved numerically using efficient finite difference procedures and ordinary differential equation solvers capable of handling variable or a priori unknown stiffness. Numerous one-dimensional as well as three-dimensional model simulations and sensitivity analyses were performed in order to test the model behavior. The results revealed that interactions between suspended virus and colloid particles can significantly affect virus transport in porous media. Previously published data from various cotransport experiments employing MS2, ΦX174, KGa-1b and STx-1b were successfully fitted by the numerical model. Consequently, the numerical model captures most of the physicochemical processes that take place during virus and colloid cotransport in porous media.

Acknowledgments

References

[1] Syngouna VI, Chrysikopoulos CV. Cotransport of clay colloids and viruses in water saturated porous media. Colloids Surf A: Physicochem Eng Aspects 2013;416:56–65. http://dx.doi.org/10.1016/j.colsurfa.2012.10.018.

[2] Reynolds KA, Mena KD, Gerba CP. Risk of waterborne illness via drinking water in the United States. Rev Environ Contam Toxicol 2008;192:117–58.

[3] Fong T, Mansfield L, Wilson D, Schwab D, Molloy S, Rose J. Massive microbiological groundwater contamination associated with a waterborne outbreak in Lake Erie, South Bass Island, Ohio. Environ Health Perspect 2007;115(6):856–64. http://dx.doi.org/10.1289/ehp.9430.

[4] Craun GF, Brunkard JM, Yoder JS, Roberts VA, Carpenter J, Wade T, Calderon RL, Roberts JM, Beach MJ, Roy SL. Causes of outbreaks associated with drinking water in the United States from 1971 to 2006. Clin Microbiol Rev 2010;23(3):507–28. http://dx.doi.org/10.1128/CMR.00077-09.

[5] Jin Y, Flury M. Fate and transport of viruses in porous media. Adv Agron 2002;77:39–102.

[6] Zhuang J, Jin Y. Virus retention and transport through Al-coated sand columns: effects of ionic strength and composition. J Contam Hydrol 2003;60:193–209.

[7] Chu Y, Jin Y, Baumann T, Yates MV. Effect of soil properties on saturated and unsaturated virus transport through columns. J Environ Qual 2003;32:2017–25.

[8] Keller AA, Sirivithayapakorn SS, Chrysikopoulos CV. Early breakthrough of colloids and bacteriophage MS2 in a water-saturated sand column. Water Resour Res 2004;40:W08304. http://dx.doi.org/10.1029/2003WR002676.

[9] Anders R, Chrysikopoulos CV. Evaluation of the factors controlling the time-dependent inactivation rate coefficients of bacteriophage MS2 and PRD1. Environ Sci Technol 2006;40(10):3237–42. http://dx.doi.org/10.1021/es051604b.

[10] Grolimund D, Borkovec M. Release of colloidal particles in natural porous media by monovalent and divalent cations. J Contam Hydrol 2006;87:155–75.

[11] Tong M, Johnson WP. Colloid population heterogeneity drives hyperexponential deviation from classic filtration theory. Environ Sci Technol 2007;41:493–9.

[12] Anders R, Chrysikopoulos CV. Transport of viruses through saturated and unsaturated columns packed with sand. Transp Porous Media 2009;76:121–38. http://dx.doi.org/10.1007/s11242-008-9239-3.

[13] Kim HN, Bradford SA, Walker SL. Escherichia coli O157:H7 transport in saturated porous media: role of solution chemistry and surface macromolecules. Environ Sci Technol 2009;43:4340–7.

[14] Chrysikopoulos CV, Masciopinto C, La Mantia R, Manariotis ID. Removal of biocolloids suspended in reclaimed wastewater by injection in a fractured aquifer model. Environ Sci Technol 2010;44(3):971–7. http://dx.doi.org/10.1021/es902754n.

[15] Ma H, Johnson WP. Colloid retention in porous media of various porosities: predictions by the hemispheres-in-cell model. Langmuir 2010;26(3):1680–7. http://dx.doi.org/10.1021/la902657v.

[16] Syngouna VI, Chrysikopoulos CV. Interaction between viruses and clays in static and dynamic batch systems. Environ Sci Technol 2010;44(12):4539–44. http://dx.doi.org/10.1021/es100107a.

[17] Syngouna VI, Chrysikopoulos CV. Transport of biocolloids in water saturated columns packed with sand: effect of grain size and pore water velocity. J Contam Hydrol 2011;126:301–14. http://dx.doi.org/10.1016/j.jconhyd.2011.09.007.

[18] Vasiliadou IA, Papoulis D, Chrysikopoulos CV, Panagiotaras D, Karakosta E, Fardis M, Papavassiliou G. Attachment of *Pseudomonas putida* onto differently structured kaolinite minerals: A combined ATR-FTIR and ¹H NMR study. Colloids Surf B 2011;84(2):354–9. http://dx.doi.org/10.1016/j.colsurfb.2011.01.026.

[19] Chrysikopoulos CV, Aravantinou AF. Virus inactivation in the presence of quartz sand under static and dynamic batch conditions at different temperatures. J Hazard Mater 2012;233–234:148–57. http://dx.doi.org/10.1016/j.jhazmat.2012.07.002.

[20] Sen TK. Processes in pathogenic biocolloidal contaminants transport in saturated and unsaturated porous media: a review. Water Air Soil Pollut 2011;216:239–56.

[21] Chrysikopoulos CV, Syngouna VI. Attachment of bacteriophages MS2 and X174 onto kaolinite and montmorillonite: extended-DLVO interactions. Colloids Surf B: Biointerfaces 2012;92:74–83. http://dx.doi.org/10.1016/j.colsurfb.2011.11.028.

[22] Chrysikopoulos CV, Sim Y. One-dimensional virus transport homogeneous porous media with time dependent distribution coefficient. J Hydrol 1996;185:199–219. http://dx.doi.org/10.1016/0022-1694(95)02990-7.

[23] McDowell-Boyer LM, Hunt JR, Sitar N. Particle transport through porous media. Water Resour Res 1986;22:1901–21.

[24] Gschwend PM, Backhus DA, MacFarlane JK, Page AL. Mobilization of colloids in groundwater due to infiltration of water at a coal ash disposal site. J Contam Hydrol 1990;6:307–20.

[25] Ronen D, Magaritz M, Weber U, Amiel AI, Klein E. Characterization of suspended particles collected in groundwater under natural gradient flow conditions. Water Resour Res 1992;28:1279–91.

[26] Compere F, Porel G, Delay F. Transport and retention of clay particles in saturated porous media: influence of ionic strength and pore velocity. J Contam Hydrol 2001;49:1–21.

[27] Mills WB, Liu S, Fong FK. Literature review and model (COMET) for colloid/metals transport in porous media. Ground Water 1991;29:199–208.

[28] Abdel-Salam A, Chrysikopoulos CV. Analysis of a model for contaminant transport in fractured media in the presence of colloids. J Hydrol 1995;165:261–81. http://dx.doi.org/10.1016/0022-1694(94)02675-2.

[29] Ouyang Y, Shinde D, Mansell RS, Harris W. Colloid enhanced transport of chemicals in subsurface environments: a review. Crit Rev Environ Sci Technol 1996;26:189–204.

[30] Saiers JE, Hornberger GM. The role of colloidal kaolinite in the transport of cesium through laboratory sand columns. Water Resour Res 1996;32(1):33–41.

[31] McCarthy JF. Colloid-facilitated transport of contaminants in groundwater: mobilization of transuranic radionuclides from disposal trenches by natural organic matter. Phys Chem Earth 1998;23:171–8.

[32] Kersting AB, Efurd DW, Finnegan DL, Rokop DJ, Smith DK, Thompson JL. Migration of plutonium in ground water at the Nevada test site. Nature 1999;397:56–9. http://dx.doi.org/10.1038/16231.

[33] Kretzschmar R, Borkovec M, Grolimund D, Elimelech M. Mobile subsurface colloids and their role in contaminant transport. Adv Agron 1999;66:121–94.

[34] Tatalovich ME, Lee KY, Chrysikopoulos CV. Modeling the transport of contaminants originating from the dissolution of DNAPL pools in aquifers in the presence of dissolved humic substances. Transp Porous Media 2000;38(1/2):93–115. http://dx.doi.org/10.1023/A:1006674114600.

[35] Maxwell R, Welty C, Harvey R. Revisiting the Cape Cod bacteria injection experiment using a stochastic modeling approach. Environ Sci Technol 2007;41(15):5548–58.

[36] Villholth KG, Jarvis NJ, Jacobsen OH, de Jonge H. Field investigations and modeling of particle-facilitated pesticide transport in microporous soil. J Environ Qual 2000;29:1298–309.

[37] McGechan MB, Lewis DR. Transport of particulate and colloid sorbed contaminants through soil: Part 1. General principles. Biosyst Eng 2002;83:255–73.

[38] Artinger R, Rabung T, Kim JI, Sachs S, Schmeide K, Heise KH, Bernhard G, Nitsche H. Humic colloid-borne migration of uranium in sand columns. J Contam Hydrol 2002;58:1–12.

[39] de Jonge LW, Moldrup P, Rubaek GH, Schelde K, Djurhuus J. Particle leaching and particle-facilitated transport of phosphorous at the field scale. Vadose Zone J 2004;3(15):462–70.

[40] James SC, Bilezikjian TK, Chrysikopoulos CV. Contaminant transport in a fracture with spatially variable aperture in the presence of monodisperse and polydisperse colloids. Stochastic Environ Res Risk Assess 2005;19(4):266–79. http://dx.doi.org/10.1007/s00477-004-0231-3.

[41] Pang L, Noonan M, Flintoft M, van den Brink P. A laboratory study of bacteria-facilitated cadmium transport in alluvial gravel aquifer media. J Environ Qual 2005;34:237–47.

[42] Sen TK, Khilar KC. Review on subsurface colloids and colloid-associated contaminant transport in saturated porous media. Adv Colloid Interface Sci 2006;119:71–96.

[43] Mibus J, Sachs S, Pfingsten W, Nebelung C, Bernhard G. Migration of uranium (IV)/(VI) in the presence of humic acids in quartz sand: a laboratory column study. J Contam Hydrol 2007;89:199–217.

[44] Severino G, Cvetkovic V, Coppola A. Spatial moments for colloid-enhanced radionuclide transport in heterogeneous aquifers. Adv Water Res 2007;30:101–12.

[45] Tien NC, Jen CP. Analytical modeling for colloid facilitated transport of *n*-member radionuclides chains in the fractured rock. Nucl Sci Tech 2007;18(6):336–43.

[46] Walshe GE, Pang L, Flury M, Close ME, Flintoft M. Effects of pH, ionic strength, dissolved organic matter, and flow rate on the cotransport of MS2 bacteriophages with kaolinite in gravel aquifer media. Water Res 2010;44:1255–69.

[47] Harvey RW, Garabedian SP. Use of colloid filtration theory in modeling movement of bacteria through a contaminated sandy aquifer. Environ Sci Technol 1991;25:178–85.

[48] Tim US, Mostaghimi S. Model for predicting virus movement through soils. Ground Water 1991;29(2):251–9.

[49] Park N, Blanford TN, Huyakorn PS. VIRALT: a modular semi-analytical and numerical model for simulating viral transport in ground water. In: International ground water modeling center, Colorado School of Mines: Golden, CO; 1992.

[50] Abdel-Salam A, Chrysikopoulos CV. Analytical solutions for one-dimensional colloid transport in saturated fractures. Adv Water Resour 1994;17(5):283–96. http://dx.doi.org/10.1016/0309-1708(94)90032-9.

[51] Sim Y, Chrysikopoulos CV. Analytical models for one-dimensional virus transport in saturated porous media. Water Resour Res. 1995;31(5):1429–37. http://dx.doi.org/10.1029/95WR00199 (Correction, Water Resour Res 32(5) 1473, 1996. http://dx.doi.org/10.1029/96WR00675).

[52] James SC, Chrysikopoulos CV. Transport of polydisperse colloid suspensions in a single fracture. Water Resour Res 1999;35(3):707–18. http://dx.doi.org/10.1029/1998WR900059.

[53] James SC, Chrysikopoulos CV. Analytical solutions for monodisperse and polydisperse colloid transport in uniform fractures. Colloids Surf A 2003;226:101–18. http://dx.doi.org/10.1016/S0927-7757(03)00316-9.

[54] Chrysikopoulos CV, James SC. Transport of neutrally buoyant and dense variably sized colloids in a two-dimensional fracture with anisotropic aperture. Transp Porous Media 2003;51:191–210. http://dx.doi.org/10.1023/A:1021952226861.

[55] Bradford SA, Torkzaban S, Simunek J. Modeling colloid transport and retention in saturated porous media under unfavorable attachment conditions. Water Resour Res 2011;47:W10503. http://dx.doi.org/10.1029/2011WR010812.

[56] Chrysikopoulos CV, Syngouna VI, Vasiliadou IA, Katzourakis VE. Transport of *Pseudomonas putida* in a three-dimensional bench scale experimental aquifer. Transp Porous Media 2012;94:634–5. http://dx.doi.org/10.1007/s11242-012-0015-z.

[57] Abdel-Salam A, Chrysikopoulos CV. Modeling of colloid and colloid-facilitated contaminant transport in a two-dimensional fracture with spatially variable aperture. Transp Porous Media 1995;20(3):197–221. http://dx.doi.org/10.1007/BF01073172.

[58] Corapcioglu MY, Kim S. Modeling facilitated contaminant transport by mobile bacteria. Water Resour Res 1995;31(11):2639–47. http://dx.doi.org/10.1029/95WR02183.

[59] Pang L, Simunek J. Evaluation of bacteria-facilitated cadmium transport in gravel columns using HYDRUS colloid-facilitated solute transport model. Water Resour Res 2006;42:W12S10. http://dx.doi.org/10.1029/2006WR004896.

[60] Bekhit HM, El-Kordy MA, Hassan AE. Contaminant transport in groundwater in the presence of colloids and bacteria, Model development and verification. J Contam Hydrol 2009;108:152–67. http://dx.doi.org/10.1016/j.jconhyd.2009.07.003.

[61] Vasiliadou IA, Chrysikopoulos CV. Cotransport of *Pseudomonas putida* and kaolinite particles through water saturated columns packed with glass beads. Water Resour Res 2011;47:W02543. http://dx.doi.org/10.1029/2010WR009560.

[62] Sim Y, Chrysikopoulos CV. Three-dimensional analytical models for virus transport in saturated porous media. Transp Porous Med. 1998;30:87–112. http://dx.doi.org/10.1023/A:1006596412177.

[63] Sim Y, Chrysikopoulos CV. Analytical solutions for solute transport in saturated porous media with semi-infinite or finite thickness. Adv Water Resour 1999;22(5):507–19. http://dx.doi.org/10.1016/S0309-1708(98)00027-X.

[64] Chrysikopoulos CV, Roberts PV, Kitanidis PK. One-dimensional solute transport in porous media with partial well-to-well recirculation: application to field experiments. Water Resour Res 1990;26(6):1189–95. http://dx.doi.org/10.1029/89WR03629.

[65] Shamir UY, Harleman DRF. Numerical solutions for dispersion in porous mediums. Water Resour Res 1967;3(2):557–81.

[66] Schenk O, Gärtner K. Solving unsymmetric sparce systems of linear equations with PARADISO. J. Future Gener Comput Syst 2004;20(3):475–87.

[67] Doherty J. PEST: software for model-independent parameter estimation. Australia: Watermark Numerical Computing; 2005.

[68] Ratha DN, Hari Prasad KS, Ojha CSP. Analysis of virus transport in groundwater and identification of transport parameters. Pract Periodical Hazard Toxic Radioactive Waste Manage 2009;13(2):98–109. http://dx.doi.org/10.1061/(ASCE)1090-025X.

[69] Sim Y, Chrysikopoulos CV. One-dimensional virus transport in porous media with time dependent inactivation rate coefficients. Water Resour Res 1996;32(8):2607–11. http://dx.doi.org/10.1029/96WR01496.